Scripta Materialia 203 (2021) 114090

Contents lists available at ScienceDirect

Scripta Materialia

journal homepage: www.elsevier.com/locate/scriptamat

In situ TEM investigation of hexagonal WO_3 irreversible transformation to Li_2WO_4

Zhenhua Wang[a], Guoxin Chen[a], Hongliang Zhang[a,*], Lingyan Liang[a], Junhua Gao[a], Hongtao Cao[a,b,*]

[a] Laboratory of Advanced Nano Materials and Devices, Ningbo Institute of Materials Technology and Engineering, Chinese Academy of Sciences, Ningbo 315201, China

[b] Center of Materials Science and Optoelectronics Engineering, University of Chinese Academy of Sciences, Beijing 100049, China

ARTICLE INFO

Article history:
Received 31 March 2021
Revised 25 May 2021
Accepted 10 June 2021

Keywords:
Tungsten oxide
Irreversible transformation
Lithium tungstate
In situ transmission electron microscopy

ABSTRACT

Lithium-ion migration at the WO_3/electrolyte interface is governed by the phase transformation mechanism by which metastable states are replaced from one phase to another. Herein, an *in situ* single nanowire-based cell is constructed to investigate the dynamic phase transformation and morphology evolution of h-WO_3 nanowire in real-time during its deep lithiation. One of the most significant features of h-WO_3 lithiation is the irreversible transformation from h-WO_3 to Li_2WO_4. There are a large number of deep ion-trapping sites composed of 4 O atoms in Li_2WO_4 crystal structure, that is, inserted lithium ions are irreversibly bound in these traps and nearly cannot be deintercalated. A mechanism on irreversible WO_3-to-Li_2WO_4 transformation in deep lithiation reaction is demonstrated. With the aid of *in situ* transmission electron microscopy, we controllably triggered lithium-ion migration at the WO_3/electrolyte interface and directly visualized the nanoscale lithium-ion migration as a stop motion movie.

Tungsten oxide (WO_3) shows a wide range of applications in electrochromic devices [1–3], lithium-ion batteries [4], fuel cells [5], and photoanodes in organic chemicals [6] due to its unique contribution to ion / proton transport properties [7]. It is generally believed that as far as electrochromic devices and lithium-ion batteries are concerned, electrodes with nanocrystals and nanostructures can increase the effective contact area of the material/electrolyte interface and improve the charge transport and lithium-ion diffusion efficiency. Thus, nanocrystalline or nanoporous WO_3 tends to enjoy the excellent electrochromic performance (greater optical modulation and higher coloration efficiency) [8,9] and superior electrochemical characteristics (good cyclic stability and higher theoretical capacity) [10]. Lithium ions are intercalated when a suitable voltage is applied to WO_3 electrodes in electrochromic devices with reversible two-state optical transformation, resulting in the formation of colored Li_xWO_3 bronze [11]. Conversely, when the applied voltage is reversed, the deintercalation of lithium ions leads to a bleached state. Recent reports reveal that there are a series of lithium-ion-trapping positions in WO_3, and when x exceeds a limit value ~ 0.65 in Li_xWO_3, the phenomenon of conspicuous ion trapping arises [12]. When excessive lithium ions are intercalated, WO_3 at the active interface undergoes an irreversible transformation to form Li_2WO_4, which is stable phase compared with metastable Li_xWO_3. As pointed out by Hashimoto *et al*, injecting a large number of lithium ions into the WO_3 electrode can form a stable lithium tungstate (Li_2WO_4) and cause its cyclic stability degradation in electrochromic and electrochemical performance [13]. It is demonstrated that excessive lithium ions and electrons lead to the formation of irreversible Li_2WO_4, and there are only two ion states of W^{6+} and W^{4+} in WO_3 electrode, which hinders the progress of the redox reaction and degrades its electrochromic performance [14]. Although such degradation originated theoretically from Li_2WO_4 has been widely considered, designing *in situ* strategy to uncover the dynamic phase transformation and morphology evolution of WO_3 electrode in real-time during its deep lithiation still needs to be experimentally explored further.

In this work, *in situ* HRTEM direct observation of hexagonal WO_3 (h-WO_3) irreversible transformation to Li_2WO_4 is conducted in an electrochemical cell setup shown in Fig. 1a, which consisted of a h-WO_3 nanowire cathode, a naturally-grown Li_2O solid electrolyte, and a bulk lithium metal counter electrode, similar to that described in the literature [15–17]. Investigation on the real-time phase transition, dynamic morphology evolution, electrochemical reaction kinetics and microscopic mechanism of h-WO_3 irreversible transformation to Li_2WO_4 via *in situ* TEM is performed.

* Corresponding author.
E-mail addresses: zhanghl@nimte.ac.cn (H. Zhang), h_cao@nimte.ac.cn (H. Cao).

https://doi.org/10.1016/j.scriptamat.2021.114090
1359-6462/

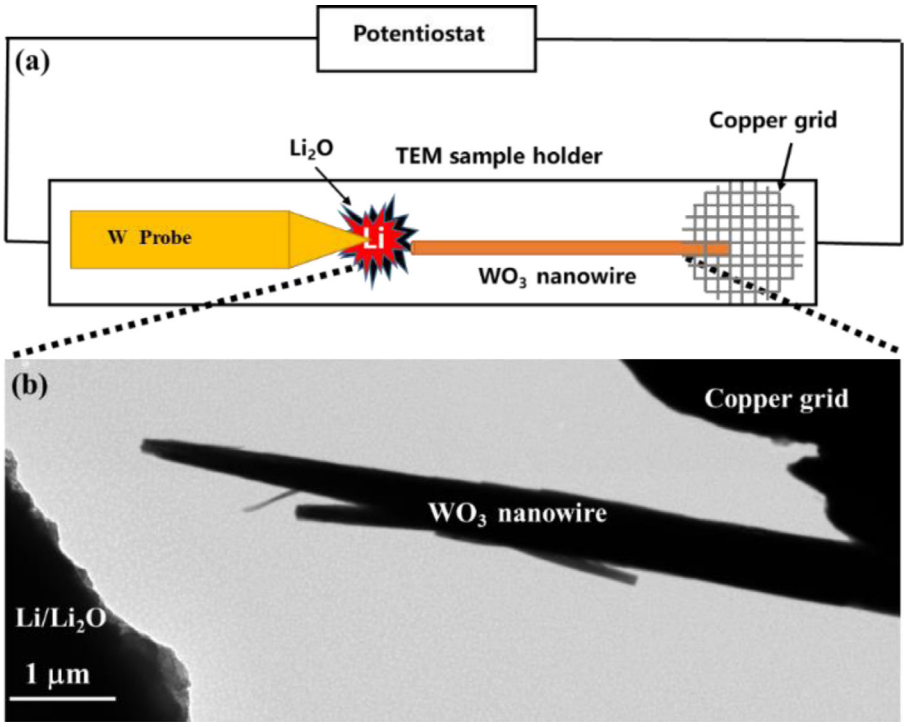

Fig. 1. (a) Schematic illustration of the *in situ* WO_3 nanowire cell. A WO_3 nanowire is bridged between copper grid current collector (right) and lithium metal with a layer of naturally-grown Li_2O (left). (b) Typical TEM image of "nanowire cell".

Fig. 1 displays a schematic illustration of the *in situ* WO_3 nanowire cell and its typical TEM image. Lithiation reaction of a single h-WO_3 nanowire was carried out under an external bias (-2.0 V). The h-WO_3 nanowires were synthesized by a facile hydrothermal method as reported elsewhere (see Experimental Section and Fig. S1 in Supplementary Materials [18]. The diameter and length of the WO_3 nanowires are varied from 150 to 300 nm and 3 to 10 μm, respectively.

Fig. 2(a) and (b) present the BF-TEM image of the pristine and lithiated state for a single WO_3 nanowire. When the nanowire cell is driven (placing a single WO_3 nanowire in intimate physical contact with Li_2O and applying an external -2.0 V voltage), the lithiation reaction occurs in the contact zone between the Li_2O thin layer and the pristine WO_3 nanowire. After the lithiation reaction is completely stopped, a lithiated layer is formed on the surface of the WO_3 nanowire, which causes an average expansion in ab-plane direction by 24.7% (see Fig. S3 and Table S1 for details). Furthermore, the lithiation diffusion distance along the c-axis direction reaches 5 μm, which is 100 times more than the diameter in the ab-plan direction. It is revealed that an anisotropic behavior of lithium-ion migration in $LiFePO_4$ is similarly observed [19]. Interestingly, a significant difference of the electrochromic switching time of the h-WO_3 nanowire array films between the perpendicular to the substrate ($t_{colored}$=30.0 s, $t_{bleached}$=17.0 s) [20] and the evenly lying on the substrate ($t_{colored}$ =272.0 s, $t_{bleached}$=364.0 s) [21] can be attributed to anisotropy of lithium-ion migration. The enlarged TEM image and selected area electron diffraction (SAED) pattern (inset) of the pristine and lithiated WO_3 nanowire are given in Fig. 2(c) and (d). The transformation from the initial h-WO_3 (JCPDS card No: 75-2187) to hexagonal Li_2WO_4 (JCPDS card No: 72-0086) during the lithiation of WO_3 nanowire is observed. In fact, when a series of external positive voltages (+2.0 V, +5.0 V, or even +10.0 V) are applied for half an hour, Li_2WO_4 is not reversibly converted to h-WO_3, which indicates the irreversible transformation from Li_2WO_4 to WO_3. In the verification experiment of the ex-situ lithium-ion battery, a relatively poor coulombic efficiency of 40.1 % is observed in the initial cycle of galvanostatic charge/discharge (GCD), which indicates the formation of stable Li_2WO_4 phase in WO_3 electrodes (Fig. S4). Fig. 2(e) shows a high-resolution TEM image of lithiation region marked by a green dotted circle in Fig. 2(d). The inverse Fast Fourier Transform (FFT) method based on *Digital Micrograph* has been applied to filter the square area 1-3, as shown in Fig. 2f–h. There are lattice fringes with 0.409 nm and 0.274 nm lattice spacing in the HRTEM image of green dashed square area 1 and 3, and pairs of bright spots can be observed in the related FFT image, corresponding to the (300) and $(23\bar{1})$ planes of Li_2WO_4, respectively. It is generally believed that the production of Li_2WO_4 in deep lithiation is apparently harmful to electrochromic devices. Operating below the threshold voltage should be considered as an effective strategy to efficiently suppress / eliminate the formation of Li_2WO_4 [14]. Besides, our previous findings suggest that synergistic effects of Li^+ and H^+ on WO_3 electrode could also inhibit the formation of Li_2WO_4 [22]. Additionally, only the halo background and no lattice fringes are found in the HRTEM image of green dashed square area 2 in the FFT image (Fig. 2(g)), implying that the lithiated layer is partly composited of a mixed amorphous phase.

To further reveal the dynamic deep lithiation process of the single h-WO_3 nanowire, time series BF-TEM images are shown in Fig. 3 (see Movie S1 for details). The series of BF-TEM images indicate that the whole lithiation reaction of the single h-WO_3 nanowire can be described as a three-stage process. In the in-situ TEM observations, no obvious changes in morphology and structure are observed during the initial electron beam irradiation process. Under the action of sufficient potential of -2.0 V, several bubble-shaped 'lithium bubbles' composed of Li^+ and Li_2O are considered to be gradually formed in the solid-state electrolyte in the first stage (Fig. 3(a)–(c)). After that, these generated 'lithium bubbles' can be migrated from Li_2O (marked by the yellow arrow in Fig. 3(b)) with a potential barrier of 0.4 eV to the outer surface of the single WO_3 nanowire (see yellow arrow in Fig. 3(c)) under the applied electric field [23]. In the second stage (Fig. 3(d)–

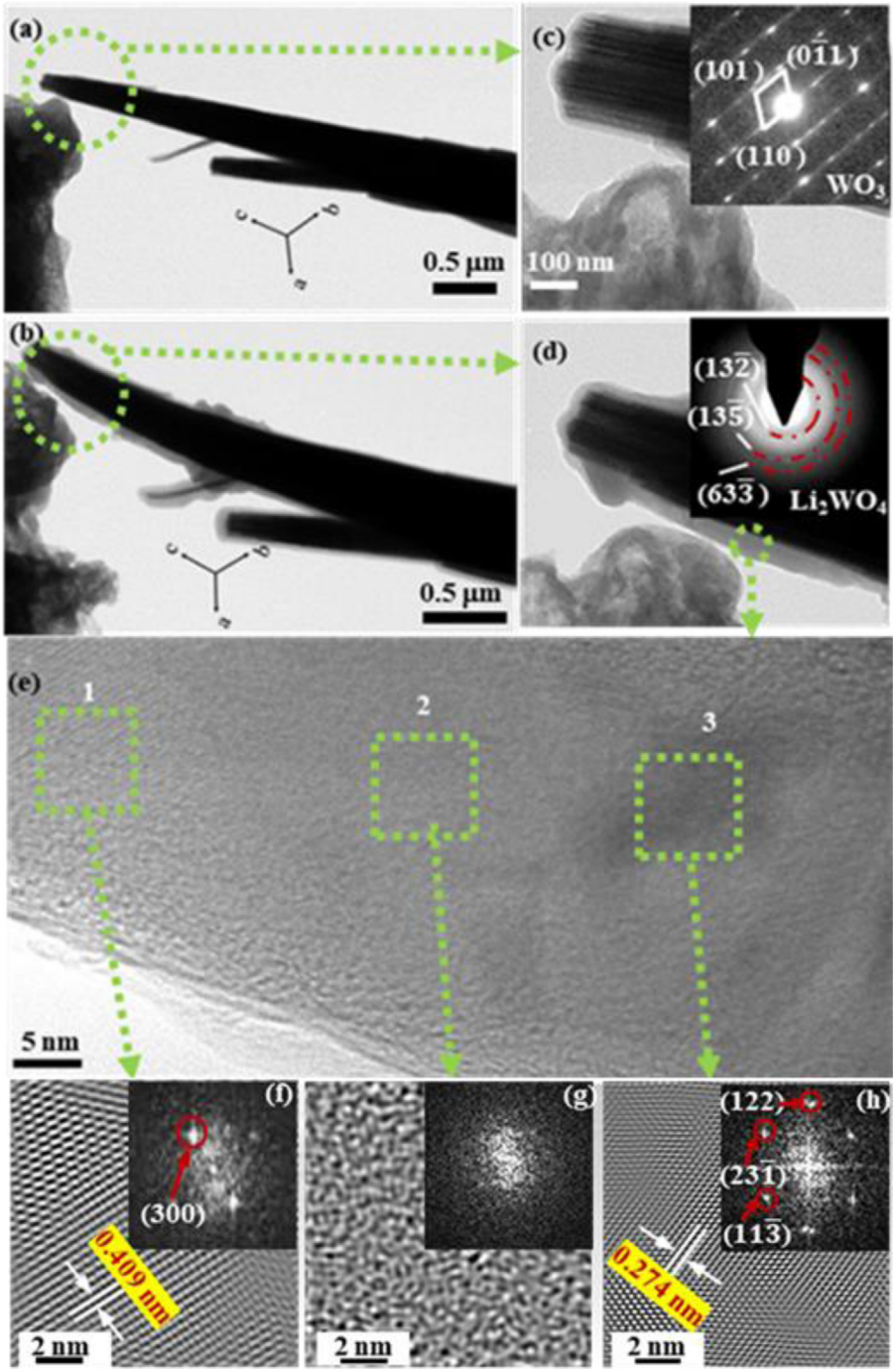

Fig. 2. Detailed structural characterization of the pristine and lithiated state for a single WO_3 nanowire. (a) Bright-field TEM (BF-TEM) image of pristine WO_3 nanowire. (b) BF-TEM image of lithiated WO_3 nanowire. (c) The enlarged TEM image and selected area electron diffraction (SAED) pattern (inset) of the pristine WO_3 nanowire. (d) The enlarged TEM image and SAED pattern (inset) of the lithiated WO_3 nanowire. (e) The high-resolution TEM (HRTEM) image of the lithiation layer, marked by a green dotted circle. (f)–(h) The inverse Fast Fourier Transform (FFT) filtered HRTEM images and FTT patterns (inset) of the characteristic region of the lithiation layer.

(g)), excessive Li^+ ions from 'lithium bubbles' can be diffused into the internal structural framework of h-WO_3. And a dynamic structural rearrangement in h-WO_3 contributes to the irreversible formation of Li_2WO_4, which gradually cause the volume expansion of the WO_3 nanowire. As the number of 'lithium bubbles' increases, the speed of the lithiation reaction has been improved greatly. During the deep lithiation of the h-WO_3 nanowire, the contact point between the lithium source and the nanowire (marked by an orange triangle) is shifted to the left by 150 nm (Fig. 3(f) and (g)), suggestive of elongation of the single h-WO_3 nanowire along c-axis, which can be due to the partial transformation from W-O-W bonds with the bond length of 3.889 Å to W-O-Li-O-Li-O-W bonds with the bond length of 9.602 Å along c-axis (Fig. S2). The volume expansion of the h-WO_3 nanowire gradually slows down with decreasing the 'lithium bubbles' and then stops, possibly predicting the occurrence and termination of its lithiation reaction in the last stage (Fig. 3(h) and (i)). The lithiated layer is acted as a passivation layer on the surface of the WO_3 electrode [24], that is to say that it can isolate the 'lithium bubbles' and the WO_3 nanowire and inhibits the further lithiation of WO_3. It is worth noting that

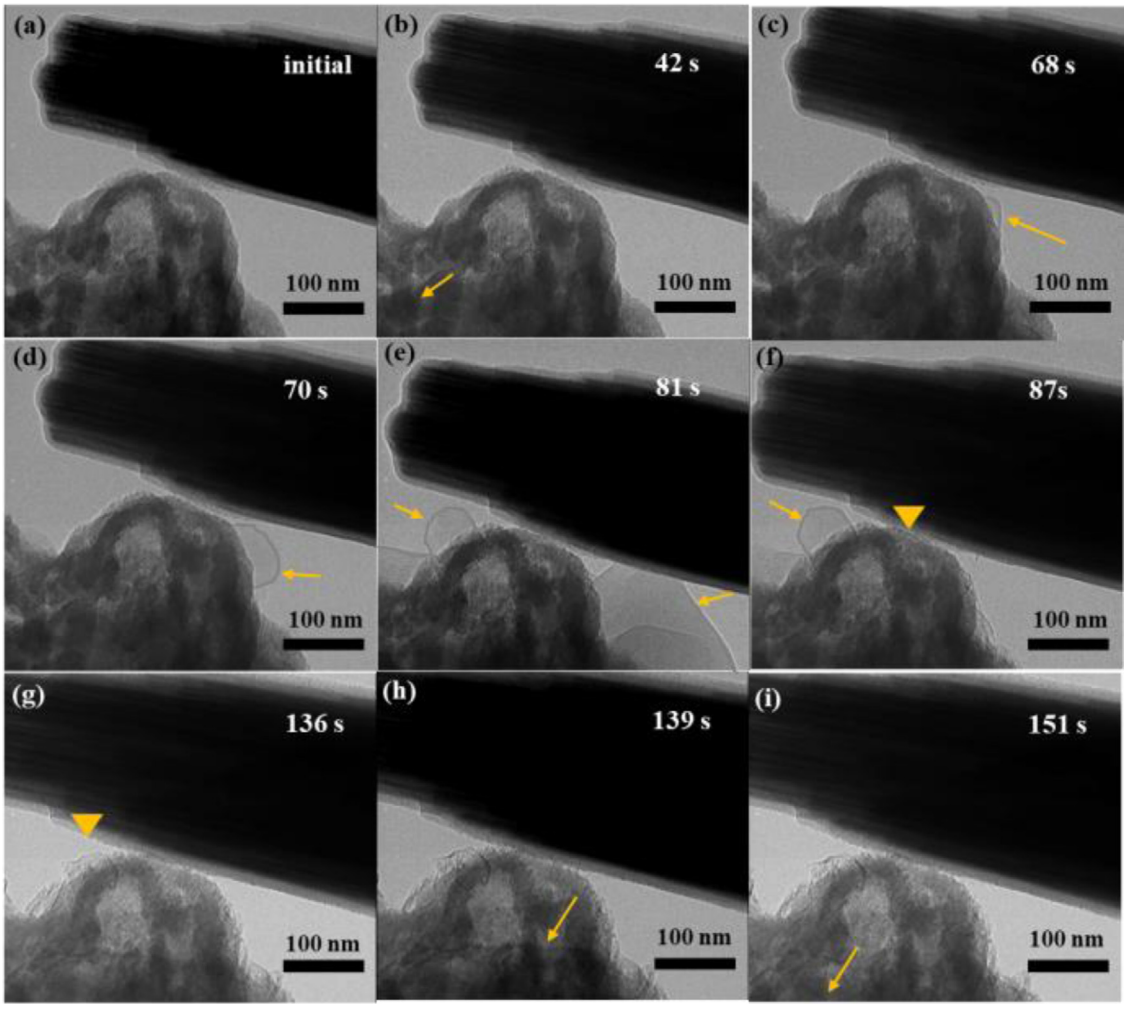

Fig. 3. Time series BF-TEM images of a single WO_3 nanowire during the lithiation process (under an external constant voltage of -2.0 V).

the generation of 'lithium bubbles' is a necessary process for the 'lithium bubbles' migration of the WO_3/electrolyte interface, and its lithiation rate seems to depend on the number of 'lithium bubbles'.

In order to explain the mechanism of irreversible transformation of h-WO_3 to Li_2WO_4, the schematic diagram of the structural transition process during the deep lithiation of the single nanowire is shown in Fig. 4. In the initial activation phase, it can be seen that 'lithium bubbles' as a lithium source (Li and Li_2O) show the fluidity characteristics of the liquid. Moreover, the solid-state 'lithium bubbles' can form a liquid-like substance driven by an external -2.0 V electric field, and it covers the outer surface of the WO_3 nanowire. Then, the excellent surface-wetting effect between the 'nanobubbles' and the single WO_3 nanowire leads to rapid and sufficient diffusive infiltration of 'lithium bubbles' into the nanowires. Lithium ions are migrated from 'lithium bubbles' (Li-rich region) to WO_3 nanowire (Li-poor region) through the 'lithium bubbles'/WO_3 interface. From the top and side view of h-WO_3 crystal structure (space group: P 6/m m m), it can be seen that there are hexagonal windows and triangular cavities along the c-axis direction and quadrilateral square windows in the ab-plane direction [25–28]. Lithium ions can be transported in all of these structural frames during the lithiation of h-WO_3 nanowire and be stored in the triangular cavities through the transportation in hexagonal windows and quadrilateral square windows [29]. For the deintercalation of lithium ions, this process follows the ordering rule that lithium ions first move from the triangular cavities to the quadrilateral square windows, then to the hexagonal windows, and finally deintercalate from WO_3. With the progress of the WO_3 lithiation reaction, lithium ions are continuously accumulated in WO_3 and reach equilibrium with that in the Li bubbles, which leads to the cessation of the lithiation reaction. The structure of WO_3 is restructured but still based on the original structure during its lithiation. In the restructuring phase, the hexagonal WO_3 composed of WO6 octahedrons is transformed into Li_2WO_4 consisted of type I (LiO4) and II (WO4) tetrahedrons. From the top and side view of the h-Li_2WO_4 crystal structure (space group: R-3(148)), it can be discovered that the inserted lithium ions participate in forming the hexagonal window, where phase transformation can generate due to the lattice in-plane deformation in the horizontal direction and the elongation of the unit cell along the c-axis. This twisted structure in Li_2WO_4 causes the inserted lithium ions to be located in ion-trapping sites composed of 4 O atoms and suppresses the deintercalation of lithium ions. The original stable triangular cavities are transformed into unstable quadrilateral window channels during the intercalation of lithium ions into h-WO_3, which can lead to the structural damage of Li_2WO_4 crystal and generation of amorphous phase in the lithiated area due to the instability of the hexagonal window and the insertion of lithium ions. From the side view, the transformation from regular quadrilateral square window to curved hexagonal channels induced by overload lithium ions can be obtained and it can hinder the intercalation / deintercalation of

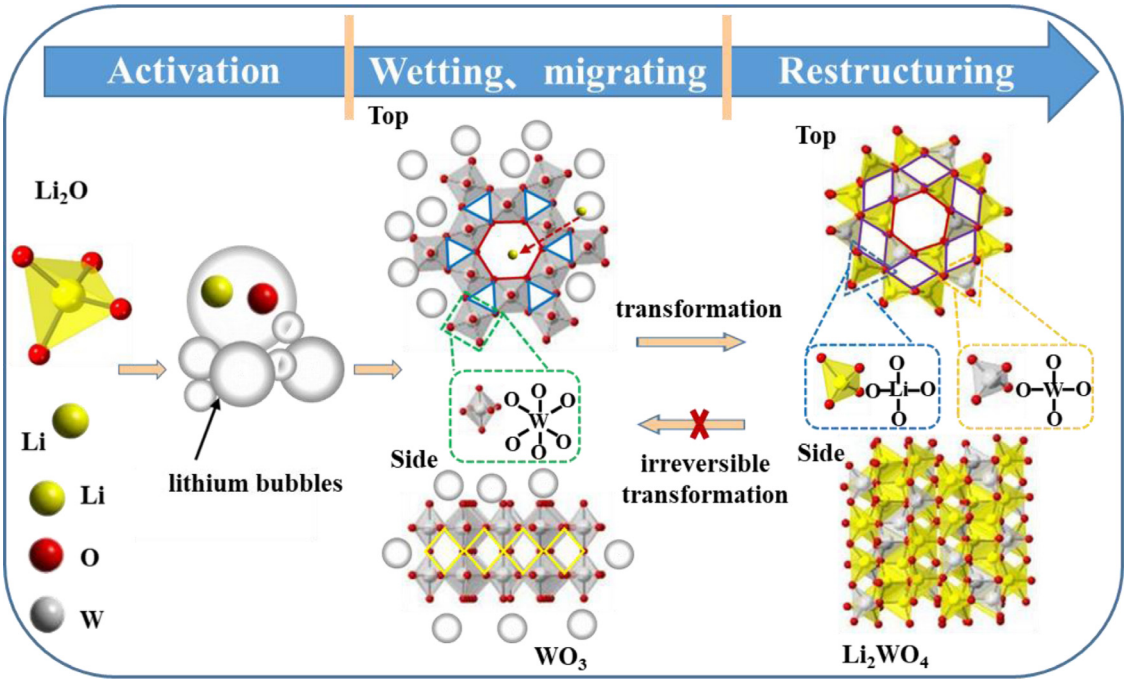

Fig. 4. Schematic diagram of the structural transformation of hexagonal WO_3 to Li_2WO_4 during the deep lithiation of a single WO_3 nanowire.

lithium ions in ab-plane direction, resulting in the lithiated layer to act as a passivation layer.

In summary, our unique experimental design demonstrates a direct observation of Li_2WO_4 irreversible transformation to h-WO_3 via *in situ* TEM. The irreversible structural transformations might widely occur in active interface kinetics such as electrochromic devices and lithium-ion batteries, which should refresh our fundamental understanding of the WO_3/electrolyte interface properties. Conventionally, the properties or the dynamic responses of the WO_3/electrolyte interface under external stimulus are considered to be only dependent on the reversible WO_3-to-Li_xWO_3 transformation. However, when the structural transformations of the WO_3 active interface occur during deep lithiation reaction, the WO_3/electrolyte interface properties should change abruptly, which suggests that the active interface properties of the WO_3 electrodes should depend on all the stable Li_2WO_4 and metastable Li_xWO_3 structures and their transformations. Moreover, our experimental approach is potentially applicable to further investigate fundamental issues of materials science that involve the WO_3/electrolyte interface dynamics.

Declaration of Competing Interest

The authors declare that they have no known competing financial interests or personal relationships that could have appeared to influence the work reported in this paper.

Acknowledgement

This project is supported by the National Natural Science Foundation of China (61974148) and Ningbo Science and Technology Innovation 2025 Major Special Project (2020Z002) .

Supplementary materials

Supplementary material associated with this article can be found, in the online version, at doi:10.1016/j.scriptamat.2021.114090.

References

[1] Y. Djaoued, S. Balaji, R. Brüning, J. Nanomater. 2012 (2012) 674168.
[2] X.T. Huo, W.G. Shen, R. Li, M. Zhang, M. Guo, Scr. Mater. 174 (2020) 1–5.
[3] V.K. Thakur, G.Q. Ding, J. Ma, P.S. Lee, X.H. Lu, Adv. Mater. 24 (2012) 4071–4096.
[4] A. Zarkadoulas, E. Koutsouri, C.A. Mitsopoulou, Coord. Chem. Rev. 256 (2012) 2424–2434.
[5] P. Balaya, Energy Environ. Sci. 1 (2008) 645–654.
[6] R. Solarska, C. Santato, C. Jorand-Sartoretti, M. Ulmann, J. Augustynski, J. Appl. Electrochem. 35 (2005) 715–721.
[7] S.H. Baeck, T. Jaramillo, G.D. Stucky, E.W. McFarland, Nano Lett. 2 (2002) 831–834.
[8] P.H. Yang, P. Sun, Z.S. Chai, L.H. Huang, X. Cai, S.Z. Tan, J.H. Song, W.J. Mai, Angew. Chem.-Int. Ed. 53 (2014) 11935–11939.
[9] S. Cong, Y.Y. Tian, Q.W. Li, Z.G. Zhao, F.X. Geng, Adv. Mater. 26 (2014) 4260–4267.
[10] B. Yang, P.X. Miao, J.Z. Cui, J. Mater. Sci.-Mater. Electron. 31 (2020) 11071–11076.
[11] C.G. Granqvist, Sol. Energy Mater. Sol. Cells 60 (2000) 201–262.
[12] R.T. Wen, C.G. Granqvist, G.A. Niklasson, Nat. Mater. 14 (2015) 996–1001.
[13] S. Hashimoto, H. Matsuoka, H. Kagechika, M. Susa, K.S. Goto, J. Electrochem. Soc. 137 (1990) 1300–1304.
[14] C.K. Wang, D.R. Sahu, S.C. Wang, C.K. Lin, J.L. Huang, J. Phys. D-Appl. Phys. 45 (2012) 225303.
[15] K. Qi, J.K. Wei, M.H. Sun, Q.M. Huang, X.M. Li, Z. Xu, W.L. Wang, X.D. Bai, Angew. Chem.-Int. Ed. 54 (2015) 15222–15225.
[16] S. Lee, Y. Oshima, E. Hosono, H.S. Zhou, K. Kim, H.M. Chang, R. Kanno, K. Takayanagi, J. Phys. Chem. C 117 (2013) 24236–24241.
[17] K. Qi, X.M. Li, M.H. Sun, Q.M. Huang, J.K. Wei, Z. Xu, W.L. Wang, X.D. Bai, E.G. Wang, Appl. Phys. Lett. 108 (2016) 233103.
[18] Y.H. Her, C.C. Chang, CrystEngComm 16 (2014) 5379–5386.
[19] Y.J. Zhu, J.W. Wang, Y. Liu, X.H. Liu, A. Kushima, Y.H. Liu, Y.H. Xu, S.X. Mao, J. Li, C.S. Wang, J.Y. Huang, Adv. Mater. 25 (2013) 5461–5466.
[20] W.G. Shen, X.T. Huo, M. Zhang, M. Guo, Appl. Surf. Sci. 515 (2020) 146034.
[21] J.M. Wang, E. Khoo, P.S. Lee, J. Ma, J. Phys. Chem. C 112 (2008) 14306–14312.
[22] K. Wang, H.L. Zhang, G.X. Chen, J. Alloys Compd. 861 (2021) 158534.
[23] X.H. Liu, J.Y. Huang, Energy Environ. Sci. 4 (2011) 3844–3860.
[24] M. Jiang, B. Key, Y.S. Meng, C.P. Grey, Chem. Mater. 21 (2009) 2733–2745.
[25] M. Hibino, W. Han, T. Kudo, Solid State Ion. 135 (2000) 61–69.
[26] S. Balaji, Y. Djaoued, A.S. Albert, R.Z. Ferguson, R. Brüning, Chem. Mat. 21 (2009) 1381–1389.
[27] K.S. Lee, D.K. Seo, M.H. Whangbo, J. Am. Chem. Soc. 119 (1997) 4043–4049.
[28] W. Han, M. Hibino, T. Kudo, Solid State Ion. 128 (2000) 25–32.
[29] J.B. Pan, Y. Wang, R.Z. Zheng, M.T. Wang, Z.Q. Wan, C.Y. Jia, X.L. Weng, J.L. Xie, L.J. Deng, J. Mater. Chem. A 7 (2019) 13956–13967.